

## LARGE-SCALE MOTIONS IN TURBULENT CHANNEL FLOW WITH SLIP CONDITION

**Min Yoon**

Dept. of Mechanical Engineering  
KAIST  
Daejeon 305-701, Korea  
minyoon@kaist.ac.kr

**Jinyul Hwang**

Dept. of Mechanical Engineering  
KAIST  
Daejeon 305-701, Korea  
j.yhwang@kaist.ac.kr

**Jin Lee**

Dept. of Mechanical Engineering  
KAIST  
Daejeon 305-701, Korea  
lee.jin@kaist.ac.kr

**Hyung Jin Sung**

Dept. of Mechanical Engineering  
KAIST  
Daejeon 305-701, Korea  
hjsung@kaist.ac.kr

**John Kim**

Dept. of Mechanical and Aerospace Engineering  
University of California, Los Angeles  
California 90095, USA  
jkim@seas.ucla.edu

### ABSTRACT

Direct numerical simulations (DNSs) of a fully developed turbulent channel flow with the slip and no-slip boundary conditions were performed to investigate the spatial characteristics of large-scale structures in the drag-reducing flow and the effect of the slip wall on those structures. The slip boundary condition was used in the streamwise direction and the overall mean skin-friction coefficient was reduced by 35% relative to the channel flow with the no-slip condition at the same bulk Reynolds number of 10,333. The wall-normal variations of average streamwise and spanwise length scales of the channel flow with the slip condition are relatively greater than those with the no-slip condition and the difference is significant in the outer region ( $y/\delta > 0.2$ ). The populations of low- and high-momentum structures are mainly due to the large populations of low-momentum structures in the channel flow with the slip condition. Based on the conditional two-point correlations, the average streamwise length scales of negative- $u$  structures in the flow with the slip condition are larger than those with the no-slip condition in the outer layer. Conditionally averaged velocity fields present that the low-momentum structures in the flow with the slip condition have the weak congregative motions and ejections, by which the near-wall streamwise velocity fluctuations are less affected.

### INTRODUCTION

The slip occurring over super-hydrophobic surfaces (SHSs) has an effect on the drag in wall-bounded turbulent flows. An air-pocket interface caused by the trapped air at grooves on the SHSs produces the free-shear regions, which leads to drag reduction via weakened mean-shear rate on the surface. With the development of nano- and micro-fabrication, studies on the SHSs have been gradually increasing to get the maximum drag reduction and to verify the mechanism of the drag reduction.

Daniello et al. (2009) experimentally showed that an optimal length scale of the ridge spacing was the viscous

sublayer thickness to obtain the super-hydrophobic surface effects when the drag reduction begun. A maximum drag reduction approximately up to 50% was obtained with streamwise grooves, which have ribs and cavities with the same spacing. Woolford et al. (2009) used the particle image velocimetry to measure the velocity profiles over the streamwise-aligned textures. They showed the lower streamwise turbulence intensity, lower Reynolds shear stress at the near-wall region, and lower turbulence production than the regular channel cases. Park et al. (2014) recently showed that the drag reduction rate was obtained up to 75% by measuring displacements between the reference- and floating-surfaces.

On the other hand, DNSs were performed for the turbulent channel flow with slip boundary conditions to mimic SHSs. Min and Kim (2004) conducted DNSs of fully developed turbulent channel flows at  $Re_\tau = 180$ , with the Navier slip boundary condition (Navier 1823) where the slip phenomena occurred entirely on the wall. When the streamwise slip occurred only, the streamwise vortices ( $\omega_x$ ) resulted in the drag-reduction performance. However, when the spanwise slip occurred, the streamwise vortices were intensified. After the pioneer work, Martell et al. (2009) considered an inhomogeneous wall condition of the turbulent channel flows with ridge and post geometries, which were modeled the side-by-side air-pocket interface. Their results were in agreement with the experimental data of  $30\mu\text{m}$  ridge spacing from Daniello et al. (2009). Park et al. (2013) executed DNSs using the streamwise grooves for SHS features at the same friction Reynolds numbers used by Martell et al. (2010). They showed that the drag reduction was constant at fixed geometry at different Reynolds numbers in laminar channel flows. However, in turbulent channel flows, the drag reduction indicated a single curve as a function of the effective slip length normalized by inner scales. The maximum drag reduction was obtained when the effective slip length in wall units was the distance of the buffer layer of turbulent channel flows. Strength of the vortical structures, which were related to the production of the Reynolds shear stress, was investigated based on the

probability density function (Jelly et al. 2014). They found that a small population of the vortical structures around the buffer layer was continuous with a decrease of the Q2 and Q4 events, which augmented turbulent drag. However, further analysis is required to explain the role of the turbulent structures on drag reduction.

Turbulent flows are composed of turbulence coherent structures having multiplicity of scales, in particular, the large-scale structures have a crucial role in the momentum transfer and the generation of turbulent kinetic energy in the outer layer (Ganapathisubramani et al., 2003; Guala et al., 2006; Balakumar and Adrian, 2007; Hutchins and Marusic, 2007; Lee and Sung, 2011). Moreover, they have an influence on the surrounding flow, especially on the near-wall streamwise velocity fluctuations. Hutchins and Marusic (2007) analyzed turbulent boundary layer flows at various friction Reynolds numbers from 1,010 to 7,300 through the single-wire spectra traverse experiments. They found that the outer peak of the long wavelength appears in the log region from the premultiplied energy spectra and these large-scales have an influence on the near-wall region as “footprint”. In addition, the large-scale structures modulate the small-scale near-wall energy (Mathis et al., 2009). They introduced the amplitude modulation coefficient, which measures the degree of the amplitude modulation of near-wall streamwise velocity fluctuations by large-scale structures.

The objectives of the present study are to investigate the spatial features of large-scale coherent structures and to compare the structures in the channel flows with the slip and no-slip conditions, for understanding about the role large-scale structures on drag reduction. The slip boundary condition can be used to determine the relative importance of the coherent structure in turbulent flow. In the present study, therefore, the DNS of the channel flow with the slip boundary condition is examined to gain the insights on drag-reduced turbulent flow. To do so, we conducted DNSs of channel flows with the slip and no-slip boundary conditions. The friction Reynolds numbers of the channel flows with the slip and no-slip conditions are 469 and 577, respectively. Structure detection method (Lee et al., 2014) is used to figure out the large-scale structures on the physical domain. The conditional two-point correlations and conditionally averaged velocities on the large-scale structures introduce to analyze the effects of the slip boundary condition on the structures.

## NUMERICAL SIMULATION

The Navier-Stokes equation and the continuity equation were used as the governing equations in this numerical study to obtain 3D flow fields of fully developed turbulent channel flows by using DNS. The governing equations are shown below:

$$\frac{\partial \tilde{u}_i}{\partial t} + \frac{\partial}{\partial x_j} \tilde{u}_i \tilde{u}_j = -\frac{\partial \tilde{p}}{\partial x_i} + \frac{1}{Re_b} \frac{\partial}{\partial x_j} \frac{\partial \tilde{u}_i}{\partial x_j} \quad (1)$$

and

$$\frac{\partial \tilde{u}_i}{\partial x_i} = 0. \quad (2)$$

Each term in the governing equations was normalized by the bulk velocity ( $U_b$ ) and the channel half-height ( $\delta$ ). The Reynolds number ( $Re_b \equiv U_b \delta / \nu$ ) was 10,333, where  $\nu$  is the kinematic viscosity. The  $x$ ,  $y$ , and  $z$  signify the streamwise, wall-normal, and spanwise directions, respectively, and the  $u$ ,  $v$ , and  $w$  present the velocity fluctuations on the corresponding directions. The upper case denote averaged quantity in both the homogeneous plane and time. The lower case represent the fluctuating quantity; e.g.,  $\overline{u}_i \equiv U_i + u_i$ .

The governing equations were solved by using the fully implicit fractional step method to decouple the velocity and pressure. The convection and viscous terms were discretized in time implicitly by using the second-order Crank-Nicolson scheme. All terms were discretized in space by using the second-order central difference scheme with the staggered grid. The details of the numerical procedure are presented in Kim et al. (2002). The periodic boundary condition was applied on the streamwise and spanwise directions. The Navier slip boundary condition (Navier 1823) ideally mimicking a super-hydrophobic surface was applied at both walls. This boundary condition are shown as  $u_s \equiv L_s (\partial u / \partial y) \big|_{\text{wall}}$ , where  $u_s$  and  $L_s$  indicate the slip velocity and slip length, respectively. The no-slip boundary condition ( $u_i = 0$ ) was also used at both walls for comparison.

The slip length was set to 0.01 to obtain the drag reduction rate of 35% at the reference channel flow with the no-slip condition. The theoretical equation, which was a function of the drag reduction rate and friction Reynolds number, from Fukagata et al. (2006) was used to determine the slip length. The friction Reynolds numbers ( $Re_\tau \equiv u_\tau \delta / \nu$ ) were 469 and 577 in the slip and no-slip boundary conditions, respectively. Note that  $u_\tau$  and  $u_{\tau 0}$  are the friction velocities of the reference channel flows with the slip and no-slip conditions, respectively. Hereafter, sub/superscript 0 means the normalized quantity by  $u_{\tau 0}$ . A very long computational domain, which was 30 times longer than the channel half-height, should be adopted to resolve the large-scale structures. The computation domain size was  $10\pi\delta \times 2\delta \times 3\pi\delta$  in the streamwise, wall-normal, and spanwise directions, respectively. The number of the grid was 2,497 ( $x$ ), 401 ( $y$ ), and 1,249 ( $z$ ) on each direction. The uniform grid spacing in the wall-parallel plane was  $\Delta x^{+0} \approx 7.27$  and  $\Delta z^{+0} \approx 4.36$ , and the grids in wall-normal direction were stretched from  $\Delta y_{\min}^{+0} \approx 0.10$  to  $\Delta y_{\max}^{+0} \approx 7.32$ . The superscript + indicates the quantity normalized by inner variables; i.e. the friction velocity  $u_\tau$  and the viscous length scale  $\delta_v$  ( $\equiv \nu / u_\tau$ ). The time steps in wall units  $\Delta t^+$  were 0.0426 and 0.0645 in the channel flows with the slip and no-slip conditions, respectively, and the total averaging time  $t_{\text{avg}}$  was about  $220\delta / U_{CL}$  on both channel flows. The current simulations with the slip and no-slip boundary conditions were performed by using 256 cores on Tachyon II (SUN B6275) and 64 cores on GAIA II (IBM p6) at the KISTI supercomputing center, respectively.

## TURBULENCE STATISTICS

Figure 1 shows the streamwise mean velocity, rms velocity fluctuations, and the Reynolds shear stress, which were normalized by the inner variables. The red and black lines represent the corresponding quantities in the channel flows with the slip and no-slip conditions, respectively. In the case of the reference channel flow with the no-slip condition (black line), the first- and second-order turbulence statistics are in good agreement with those of turbulent channel flow with  $Re_\tau = 587$  from Moser et al. (1999). The mean streamwise velocity profile in the channel flow with the slip condition, however, was shifted upward by the influence of the slip velocity. The rms of  $u$  increased at the near-wall region due to the existence of the slip velocity. After the location of the inner peak, however, the rms of  $u$  in the channel flow with the slip condition followed that with the no-slip condition.

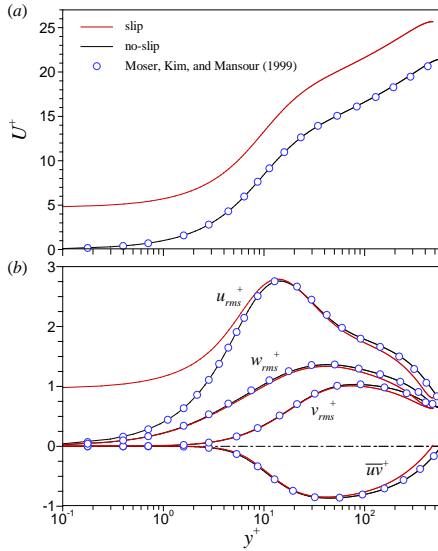


Figure 1. Wall-normal distributions of: (a) streamwise mean velocity; (b) rms velocity fluctuations and Reynolds shear stress. All quantities are normalized by the inner variables.

The two-point correlations of between the streamwise velocity fluctuations was examined to figure out the difference of the coherent structures in each channel flow. The correlation function is shown below:

$$R[u, u](\mathbf{r}, y) = \frac{\langle u(\mathbf{x}, y_{ref})u(\mathbf{x} + \mathbf{r}, y) \rangle}{u_{rms}(y_{ref})u_{rms}(y)}, \quad (3)$$

where  $\langle \cdot \rangle$  indicates the spatial and temporal averaged quantity. The characteristic streamwise length scale ( $l_x$ ) and spanwise length scale ( $l_z$ ) based on the two-point correlations with the threshold value of  $R[u, u] = 0.05$  and  $0.3$  at the reference position ( $r_x = 0$  and  $r_z = 0$ ), which is consistent with the previous work to compare the coherent structures in different flows (Lee and Sung, 2013; Sillero et al., 2014), are shown in figure 2.

The characteristic streamwise length scales of  $R[u, u] = 0.05$  in the channel flow with the slip condition grow

gradually from the wall to the core region. In the channel flow with the no-slip condition, however, the characteristic streamwise length scales are  $l_x \approx 8\delta$  consistently after  $y = 0.2\delta$ . The characteristic length scales of  $R[u, u] = 0.3$  in the channel flow with the slip condition follow the flow with the no-slip condition at all wall-normal locations with slightly higher values. The characteristic spanwise length scales widen continually toward the core region. Especially in the channel flow with the slip condition, the characteristic spanwise length scales are slightly wider than those with the no-slip condition. In the further section, the reasons of the difference of the characteristic length scales for both flows were analyzed in detail.

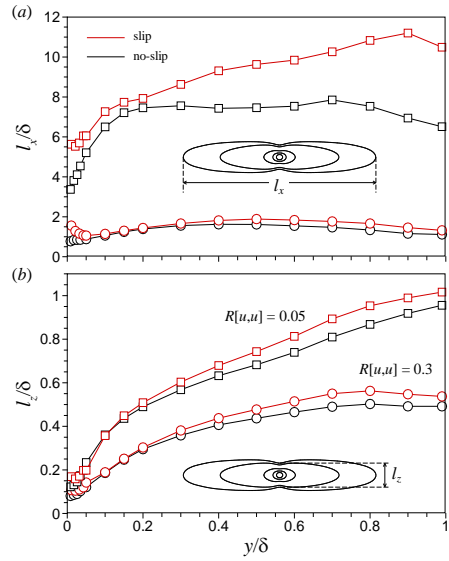


Figure 2. Variations in the characteristic (a) streamwise and (b) spanwise length scales based on the threshold values: squares,  $R[u, u] = 0.05$  and circles,  $R[u, u] = 0.3$ .

## CONDITIONAL STATISTICS

To examine the difference of the length scales observed in figure 2, the conditional sampling was conducted to figure out the large-scale structures from the physical domain. The 2D Gaussian filter and a long wavelength pass filter with the cut-off wavelength of  $1\delta$  were applied for the raw flow fields to eliminate the small-scale features. From the filtered flow field, the characteristic projections (CP) were obtained as local extrema along the  $z$ -direction which represent the streamwise length of the streamwise velocity fluctuations in the wall-parallel plane. The velocity threshold of the current detection algorithm was 10% of the bulk velocity ( $u_{th} = 0.1U_b$ ) consistent with the previous work and the details of the structure detection method are presented in Lee et al. (2014). Figure 3 displays the populations of the streamwise lengths ( $L_{CP}$ ) of the  $u$ -streaks along the wall-normal direction. Note that the populations are defined as the mean number of long  $u$ -streaks ( $L_{CP} > 1\delta$ ) in an instantaneous flow field. The streamwise lengths of the negative  $u$ -streaks in the channel flows with the slip and no-slip conditions are observed up to  $20\delta$  above. In the case of

the positive  $u$ -streaks, on the other hand, the populations are narrowly distributed below  $L_{CP} = 18\delta$ . At the inner region, the negative and positive  $u$ -streaks in the channel flow with the slip condition have larger populations than those with the no-slip condition up to  $y = 0.15\delta$ . The populations of the negative and positive  $u$ -streaks in both channel flows gradually decrease in compliance with an increase of the wall-normal location from the log region ( $y = 0.1\delta$ ) to the core region. Above all, the channel flow with the slip condition has smaller populations of the positive  $u$ -streaks than the flow with the no-slip condition. In figure 3(a), however, the populations of the negative  $u$ -streaks in the channel flow with the slip condition are larger than those with the no-slip condition in the outer region from  $0.3\delta$  to  $0.8\delta$ . The rise in the populations of long negative  $u$ -streaks ( $L_{CP} > 10\delta$ ) in the channel flow with the slip condition over  $y = 0.3\delta$  accorded with an increase in the characteristic streamwise length scales (red line) in figure 2(b).

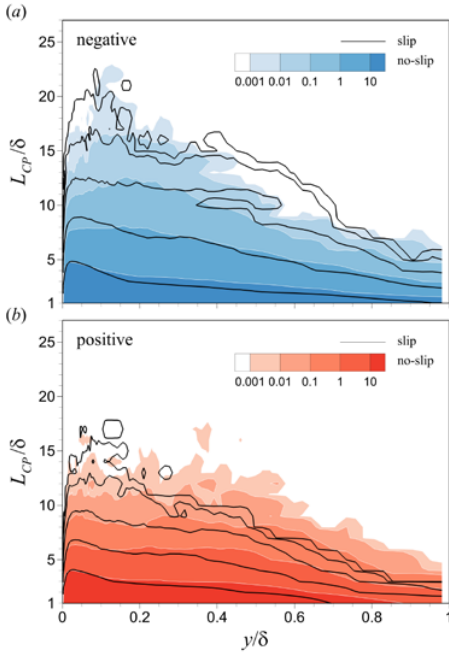


Figure 3. Populations of (a) the negative and (b) the positive  $u$ -structures ( $\geq 1\delta$ ). Line and color contours indicate the channel flows with the slip and no-slip conditions, respectively.

The statistically averaged properties of large-scale low- and high-speed events were examined using two-point correlations to investigate different population trends of those structures in the channel flows with the slip and no-slip condition. The two-point correlation is defined as,

$$R[A, B](\mathbf{r}) = \frac{\langle A(\mathbf{x})B(\mathbf{x} + \mathbf{r}) \rangle}{\langle A(\mathbf{x})B(\mathbf{x}) \rangle}, \quad (4)$$

and the conditions for the  $u$  around the long  $u$ -streaks are

$$u_{neg} = \begin{cases} u & \text{if } \hat{u} < -u_{th} \text{ and } L_{CP} > 1\delta \\ 0 & \text{otherwise} \end{cases} \quad (5)$$

and

$$u_{pos} = \begin{cases} u & \text{if } \hat{u} > +u_{th} \text{ and } L_{CP} > 1\delta \\ 0 & \text{otherwise} \end{cases}, \quad (6)$$

where  $\hat{u}$  indicates the filtered  $u$ . Figure 4 displays the conditional two-point correlations  $R[u_{neg}, u_{neg}]$  and  $R[u_{pos}, u_{pos}]$  in the wall-parallel plane. Note that the correlations are shown only half of them due to the spanwise symmetry. The characteristic spanwise length scales ( $l_z$ ) of the conditional two-point correlations are similar for both flows. The characteristic streamwise length scales ( $l_x$ ), however, have different features depending on the channel flows with the slip and no-slip conditions. In the channel flow with the slip condition, the characteristic streamwise length scales of the negative  $u$ -streaks are longer than the  $l_x$  in the channel flow with the no-slip condition as about  $0.25\delta$  and  $0.27\delta$  at  $y = 0.15\delta$  and  $y = 0.6\delta$ , respectively. The long negative coherent structures in the channel flow with the slip condition reveal the large populations of the negative  $u$ -streaks at the outer region, especially at around  $y = 0.6\delta$ . The streamwise length scales of the positive  $u$ -streaks in the slip channel also has relatively long  $l_x$  at  $y = 0.15\delta$  in connection with the large populations of the positive large-scale structures at that location. At  $y = 0.6\delta$ , however, the channel flow with the slip condition have the small characteristic streamwise length scales as about  $0.17\delta$  from the no-slip case, representing the small populations of the positive  $u$ -streaks in the channel flow with the slip condition at around  $y = 0.6\delta$  in figure 3(b). In the channel flow with the slip condition, the large populations of the negative  $u$ -streaks at the outer region (figure 3(a)) and the long negative coherent structures (figure 4(a)) induced the difference of the characteristic streamwise length scale distributions of two-point correlations for both channel flows in figure 2(a).

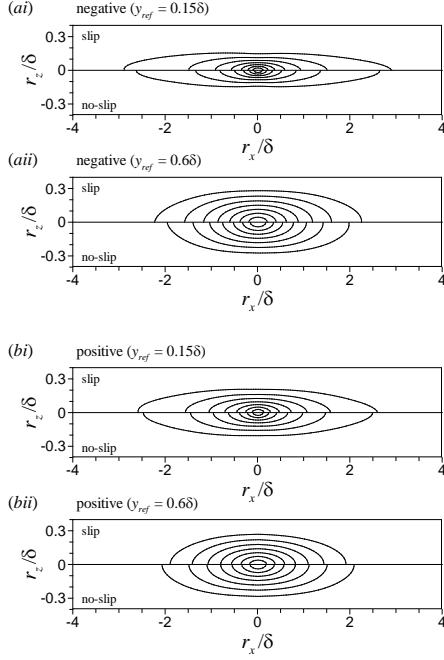


Figure 4. Two-point correlations in the wall-parallel ( $x$ - $z$ ) planes; (a) negative  $u$ -streaks ( $R[u_{neg}, u_{neg}]$ ) and (b) positive  $u$ -streaks ( $R[u_{pos}, u_{pos}]$ ) at (i)  $y = 0.15\delta$  and (ii)  $y = 0.6\delta$ . The contour levels are varied from 0.3 to 0.9 with interval of 0.1.

Using the structure-detection method, the large-scale low-speed structures were conditionally averaged to analyze the flow field around them. Figure 5 shows the conditionally averaged velocity fields based on the negative  $u$ -streaks. The left panel illustrates the perspective view of the conditionally averaged  $u$ -structures with the isosurface level at  $-0.3$  of the streamwise velocity fluctuations ( $u^{+0}$ ) and the inserted line contours represent the  $u^{+0}$  at the reference wall-normal location varied from  $-0.2$  to  $-1.0$  with an interval of  $0.2$ . The conditionally averaged  $u$ -structures in the channel flow with the slip condition have longer streamwise extend ( $6.8\delta$ ) than the no-slip case ( $5.9\delta$ ). The line contours also show the long streamwise length of the channel flow with the slip condition in the downstream. The cross-stream planes ( $r_x/\delta = 0$ ) of the conditionally averaged velocity fields are plotted in the right panel; the conditionally averaged  $w^{+0}$  with the filled contours and vectors for the spanwise and wall-normal velocity components. The filled contours vary  $-0.4$  to  $0.4$  with an increment of  $0.2$ . Although conditionally averaged patterns for both flows represent the ejections around the reference position, the low-speed structure of the no-slip channel induces the strong ejection than that of the slip channel; the maximum Reynold shear stress of the no-slip channel is  $1.46$  times larger than the slip case. The in-plane vectors at the near-wall display congregative motions under the negative large-scale structures. The channel flow with the no-slip condition have more strong congregative motions, the maximum  $w$  of the channel flow with the no-slip condition is  $1.18$  times stronger, than the slip cases. The weaker ejection events and congregative motions in the channel flow with the slip

condition relative to the no-slip cases could be induce the less modulation effects on the near-wall  $u$ .

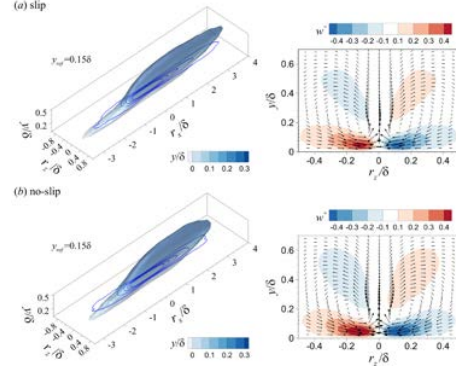


Figure 5. 3D representation of the conditionally averaged velocities and the cross-sections at  $r_x = 0$  in the channel flows with (a) the slip and (b) no-slip conditions.

## CONCLUSIONS

DNSs of fully developed turbulent channel flow with the slip boundary condition was performed. Regular turbulent channel flow with the no-slip boundary condition was also examined for comparison. The friction Reynolds numbers were  $577$  and  $490$  in the slip and no-slip boundary conditions, respectively, at the same bulk Reynolds number of  $10,333$ . The two-point correlations of the streamwise velocity showed differences of the turbulence structures between both conditions generally. To analyze the characteristics and effects of the large-scale structures, conditionally sampled velocities were applied to the turbulence statistics. The populations of the low-speed large-scales in the channel flow with the slip condition significantly increased at the outer region from  $0.4\delta$  to  $0.8\delta$ . The average streamwise length scales of the low-speed large-scale structures in the channel flow with the slip condition are larger than those with the no-slip condition in the outer region on the basis of the conditional two-point correlations. This results correspond with the high populations of the negative large-scale structures in the channel flow with the slip condition at the outer region. The conditionally averaged velocity fields in the negative  $u$ -streaks in the channel flow with the no-slip condition show that the maximum Reynolds stress and spanwise velocity fluctuations are  $1.48$  and  $1.18$  times larger, respectively, than those with the slip condition. The channel flow with the slip condition has less effect on the near-all  $u$  on account of the weak congregative motions and ejections. The large-scale coherent structures, especially the negative large-scale structures, in the channel flow with the slip condition have the different features. Future efforts will be conducted towards the effects of the negative and positive large-scale coherent structures on drag reduction for the active control of turbulence.

## ACKNOWLEDGEMENT

This work was supported by the Creative Research Initiatives (No. 2015-001828) program of the National Research Foundation of Korea (MSIP), and partially supported by the Supercomputing Center (KISTI).

## REFERENCES

- Adrian, R. J., 2007, "Hairpin vortex organization in wall turbulence", *Physics of Fluids*, Vol. 19(4), 041301.
- Balakumar, B. J., and Adrian, R. J., 2007, "Large-and very-large-scale motions in channel and boundary-layer flows" *Philosophical Transactions of the Royal Society A: Mathematical, Physical and Engineering Sciences*, Vol. 365(1852), pp. 665-681.
- Daniello, Robert J., Nicholas E. Waterhouse, and Jonathan P. Rothstein, 2009, "Drag reduction in turbulent flows over superhydrophobic surfaces", *Physics of Fluids*, Vol. 21(8), 085103.
- Fukagata, K., Kasagi, N., and Koumoutsakos, P., 2006, "A theoretical prediction of friction drag reduction in turbulent flow by superhydrophobic surfaces", *Physics of Fluids*, Vol. 18(5), 051703.
- Ganapathisubramani, B., Longmire, E. K., and Marusic, I., 2003, "Characteristics of vortex packets in turbulent boundary layers", *Journal of Fluid Mechanics*, Vol. 478, pp. 35-46.
- Guala, M., Hommema, S. E., and Adrian, R. J., 2006, "Large-scale and very-large-scale motions in turbulent pipe flow", *Journal of Fluid Mechanics*, Vol. 554, pp. 521-542.
- Hutchins, N., and Marusic, I., 2007, "Evidence of very long meandering features in the logarithmic region of turbulent boundary layers", *Journal of Fluid Mechanics*, Vol. 579, pp. 1-28.
- Jelly, T. O., Jung, S. Y., and Zaki, T. A., 2014, "Turbulence and skin friction modification in channel flow with streamwise-aligned superhydrophobic surface texture", *Physics of Fluids*, Vol. 26(9), 095102.
- Kim, K. C., and Adrian, R. J., 1999, "Very large-scale motion in the outer layer", *Physics of Fluids*, Vol. 11(2), pp. 417-422.
- Kim, K., Baek, S. J., and Sung, H. J., 2002, "An implicit velocity decoupling procedure for the incompressible Navier-Stokes equations", *International journal for numerical methods in fluids*, Vol. 38(2), pp. 125-138.
- Lee, J. H., and Sung, H. J., 2011, "Very-large-scale motions in a turbulent boundary layer", *Journal of Fluid Mechanics*, Vol. 673, pp. 80-120.
- Lee, J. H., and Sung, H. J., 2013, "Comparison of very-large-scale motions of turbulent pipe and boundary layer simulations", *Physics of Fluids*, Vol. 25(4), 045103.
- Lee, J., Lee, J. H., Choi, J. I., and Sung, H. J., 2014, "Spatial organization of large-and very-large-scale motions in a turbulent channel flow", *Journal of Fluid Mechanics*, Vol. 749, pp. 818-840.
- Martell, M. B., Perot, J. B., and Rothstein, J. P., 2009, "Direct numerical simulations of turbulent flows over superhydrophobic surfaces", *Journal of Fluid Mechanics*, Vol. 620, pp. 31-41.
- Martell, M. B., Rothstein, J. P., and Perot, J. B., 2010, "An analysis of superhydrophobic turbulent drag reduction mechanisms using direct numerical simulation", *Physics of Fluids*, Vol. 22(6), 065102.
- Mathis, R., Hutchins, N., and Marusic, I., 2009, "Large-scale amplitude modulation of the small-scale structures in turbulent boundary layers", *Journal of Fluid Mechanics*, Vol. 628, pp. 311-337.
- Min, T., and Kim, J., 2004, "Effects of hydrophobic surface on skin-friction drag", *Physics of Fluids*, Vol. 16(7), L55-L58.
- Moser, R. D., Kim, J., and Mansour, N. N., 1999, "Direct numerical simulation of turbulent channel flow up to  $Re=590$ ", *Phys. Fluids*, Vol. 11(4), pp. 943-945.
- Navier, C. L. M. H., 1823, "Mémoire sur les lois du mouvement des fluides", *Mémoires de l'Académie Royale des Sciences de l'Institut de France*, Vol. 6, pp. 389-440.
- Ou, J., Perot, B., and Rothstein, J. P., 2004, "Laminar drag reduction in microchannels using ultrahydrophobic surfaces", *Physics of Fluids*, Vol. 16(12), pp. 4635-4643.
- Park, H., Park, H., and Kim, J., 2013, "A numerical study of the effects of superhydrophobic surface on skin-friction drag in turbulent channel flow", *Physics of Fluids*, Vol. 25(11), 110815.
- Park, H., Sun, G., and Kim, C. J., 2014, "Superhydrophobic turbulent drag reduction as a function of surface grating parameters", *Journal of Fluid Mechanics*, Vol. 747, pp. 722-734.
- Sillero, J. A., Jiménez, J., and Moser, R. D., 2014, "Two-point statistics for turbulent boundary layers and channels at Reynolds numbers up to  $\delta^+ \approx 2000$ ", *Physics of Fluids*, Vol. 26(10), 105109.
- Woolford, B., Prince, J., Maynes, D., and Webb, B. W., 2009, "Particle image velocimetry characterization of turbulent channel flow with rib patterned superhydrophobic walls", *Physics of Fluids*, Vol. 21(8), 085106.